ANALYSIS OF MICROELECTROMECHANICAL SYSTEMS (MEMS) BY MESHLESS LOCAL KRIGING (LOKRIGING) METHOD

Qing Xia Wang*, Hua Li, Khin Yong Lam, and Yuan Tong Gu

ABSTRACT

A meshless Local Kriging (LoKriging) method is developed and used in this paper to analyze the behaviors of microelectromechanical system (MEMS) devices, which are simplified as thick beam systems subjected to dynamic non-linear loading induced by applied voltages. In LoKriging, the Kriging interpolation technique is employed to obtain the shape function, which has a partition of unity and delta function properties. The local Petrov-Galerkin weak form of the governing equations for MEMS devices is derived. The developed LoKriging method is used to analyze the behavior of microswitches and microtweezers, widely used for MEMS devices. Their static and dynamic characters are analyzed and compared with the results of experiments and other numerical methods. The computed results show that the present LoKriging method is easy to implement, efficient and accurate for the numerical simulation of MEMS devices. In addition, the method developed in this paper also has good potential for analysis of other complex MEMS devices.

Key Words: MEMS device, microswitch, microtweezer, meshless method, kriging interpolation, local weak form.

I. INTRODUCTION

Microelectromechanical systems (MEMS) have recently attracted a lot of attention because of numerous applications. Besides conventional fields, applications involve previously unrelated fields, such as biology and microelectronics, and their uses will continue to expand. At present, there are a few interesting applications in avionics and aerospace (microscale actuators and sensors), automotive systems (transducers and accelerometers), manufacturing and fabrication (micro smart robots), medicine and bioengineering (DNA and genetic code analysis and synthesis, drug delivery, diagnostics and imaging), etc. (Lyshevski, 2002). Among these applications, the traditional finite element methods (FEM) and computer-aided design (CAD) are the major simulation techniques. However, in the FEM analysis of some MEMS devices, the mesh generation is computationally expensive and mesh refinement is difficult, especially for problems with complicated geometries and multiple domains. In MEMS structures, the mesh generation is complicated for the following reasons:

- Multi-domain problems are usually considered because they often involve electric and mechanical domains.
- The problems analyzed are often non-linear.

In order to overcome difficulty in mesh generation, more efficient simulation methods are required (Senturia, 1998; Hung and Senturia, 1999). The recently developed meshless technique is one good alternative, because it does not require a mesh and simulation can be implemented by arbitrarily distributed nodes covering the multiple energy domains.

In the development and application of meshless methods, many researchers have made great achievements (Belytschko *et al*., 1996; Liu, 2002). A group

*Corresponding author. (Tel: +65-64191560; Fax: +65-64191380; Email: wangqx@ihpc.a-star.edu.sg)

Q. X. Wang, H. Li, and K. Y. Lam are with the Institute of High Performance Computing, 1 Science Park Road, #01-01 The Capricorn, Singapore Science Park II, Singapore 117528.

Y. T. Gu is with the Department of Mechanical Engineering, National University of Singapore, 10 Kent Ridge Crescent, Singapore 119260.

meshless methods have been developed. The developed meshless methods can be classified based on different criteria. According to the computational modeling used, they can be largely categorized into two types (Liu, 2002). One type is meshless methods based on the strong form of partial differential equations (PDEs). It includes smooth particle hydrodynamics (SPH) (Gingold and Monaghan, 1977; Monaghan, 1985), the vortex method (Leonard, 1980; Bernard, 1995) and the generalized finite difference method (Liszka, 1984), etc. The other type is based on the weak form of PDEs, including the element-free Garlerkin (EFG) method (Belytschko *et al*., 1994, 1996), the meshless local Petrov-Galerkin (MLPG) (Atluri and Zhu, 1998; Atluri *et al*., 1999a, b; Gu and Liu, 2001a), the point interpolation method (PIM) (Liu and Gu, 2001a, b; Gu and Liu, 2001b), and so on. In them, MLPG (Atluri and Zhu, 1998; Atluri *et al*., 1999a, b) and the local radial point interpolation method (LRPIM) (Liu and Gu, 2001b; Liu *et al*., 2002b) are meshless methods based on the local Petrov-Galerkin weak forms, which are used to avoid global integrations.

Among the above mentioned meshless methods, the moving least squares (MLS) and the radial point interpolation method (RPIM) are two widely used meshless interpolation techniques. Recently, researchers have tried to use the Kriging interpolation technique for construction of meshless shape functions. The Kriging is the estimation procedure originally used in geostatistics by using known values and a semivariogram to determine unknown values. It is named after Krige (1951, 1976) and has been extensively used in computer experiments (Sacks *et al*., 1989) and optimal design (Simpson *et al*., 1998). The simplified Kriging version can be found in the work of Trochu (1993). Kriging interpolation has the following advantages:

- Since the Kriging is based on the statistics for the minimum of the mean square error, it can ensure interpolation accuracy. In other words, the Kriging has a solid theoretical base to ensure desirable interpolation accuracy.
- A group of variogram models has been proposed in Kriging interpolation. For example, in (Olea, 1999), there are seven variogram models (e.g. spherical, rational quadratic, etc.). Applying one or another variogram model allows better representation of the variance in the data set.
- The Kriging interpolation is stable for arbitrary nodal distributions.
- The shape functions constructed by the Kriging interpolation possess Kronecker delta function properties.

Because of the above advantages of the Kriging interpolation, the Kriging method has found wide application in a variety of fields so far. Recently, researchers have tried to explore its possible application in meshless methods based on global weak forms (Liu *et al*., 2002a; Gu, 2003). However, this application is in the beginning stage. A lot of research is required. It should be noted that Liu *et al*. (2002a) unveiled that the Kriging interpolation will lead to the same shape functions as RPIM if the same RBF and semivariogram are adopted. However, theories and algorithms of RPIM and Kriging are completely different. RPIM and Kriging interpolation cannot replace each other. Hence, the research for the application of Kriging to meshless methods is still very significant because the Kriging method opens an alternative avenue to develop meshless methods.

In this paper, a novel meshless Local Kriging (LoKriging) method is developed for analyses of microelectromechanical system (MEMS) devices that are subjected to dynamic nonlinear loading induced by applied voltages. These MEMS devices are simplified as beam systems. The Kriging interpolation technique is employed to obtain the shape function, which has a partition of unity and delta function properties. The local Petrov-Galerkin weak form of the governing equations for MEMS devices is derived. The developed LoKriging method is used to analyze the static and dynamic behaviors of MEMS devices, the microswitch and the microtweezer. The numerical results obtained by LoKriging are compared with the results from experiments and other numerical methods. It is found that the present LoKriging method is easy to implement, efficient and accurate for the numerical simulation of MEMS devices. In addition, the method developed in this paper has also very good potential for analysis of other complex MEMS devices (e.g. devices with plate structures).

II. KRIGING INTERPOLATION FORMULATION

We consider a random function $u(\boldsymbol{x})$ defined in the domain Ω which is discretized by a set of scattered nodes $\boldsymbol{x}_i$ ($1 \le i \le N$), where N is the total number of nodes. It is assumed that only surrounding nodes of one point $\boldsymbol{x}_0$ have any effect on $u(\boldsymbol{x}_0)$. The domain that includes these surrounding nodes is defined as the interpolation domain. Then, the estimated value at point $\boldsymbol{x}_0$, $u^h(\boldsymbol{x}, \boldsymbol{x}_0)$, can be written as

$$u^h(\boldsymbol{x}, \boldsymbol{x}_0) = \sum_{i=1}^{n} \lambda_i u(\boldsymbol{x}_i) \tag{1}$$

where $u(\boldsymbol{x}_i)$ is the value at $\boldsymbol{x}_i$ (i=1, 2, ⋯, n), and n is the number of nodes in the interpolation domain of $\boldsymbol{x}_0$. λ_i is the weight assigned to the neighboring nodes.

λ_i can be determined by minimizing the squared variance of the estimation error $E\{[u(\boldsymbol{x}_0)-u^h(\boldsymbol{x}, \boldsymbol{x}_0)]^2\}$ (Trochu, 1993; Olea, 1999).

If the estimation formula (Eq. (1)) is no-bias, the expected values of $u(\boldsymbol{x}_0)$ and $u^h(\boldsymbol{x}, \boldsymbol{x}_0)$ must be identical, i.e.

$$E[u(\boldsymbol{x}_0)] = E[u^h(\boldsymbol{x}, \boldsymbol{x}_0)] = \sum_{i=1}^{n} \lambda_i E[u(\boldsymbol{x}_i)] \tag{2}$$

In Kriging, the unknown function $u(\boldsymbol{x}_0)$ is composed of two parts

$$u(\boldsymbol{x}_0)=Z_a(\boldsymbol{x}_0)+Z_b(\boldsymbol{x}_0) \tag{3}$$

where $Z_b(\boldsymbol{x}_0)$ represents a stationary fluctuation, i.e. $E[Z_b(\boldsymbol{x}_0)]=0$. $Z_a(\boldsymbol{x}_0)$, called the drift, represents the expected value of $u(\boldsymbol{x}_0)$. It is written as

$$Z_a(\boldsymbol{x}_0) = \sum_{i=1}^{n} \lambda_i Z_a(\boldsymbol{x}_i) \tag{4}$$

Usually, the drift can be chosen arbitrarily. If it is assumed that the drift belongs to a finite linear subspace S and taken as a linear polynomial, we have the form

$$\sum_{i=1}^{n} \lambda_i p_l(\boldsymbol{x}_i) = p_l(\boldsymbol{x}_0), \quad 1\le l\le k \tag{5}$$

where the basis function $p_l(\boldsymbol{x})$ is the monomial in S. In one-dimensional space, $\boldsymbol{p}^T(\boldsymbol{x})=\{1, x\}$ and in two dimensions, $\boldsymbol{p}^T(\boldsymbol{x})=\{1, x, y\}$.

Minimizing the squared variance of the estimation error, we obtain the Kriging system equation as follows:

$$\sum_{j=1}^{n} E[u(\boldsymbol{x}_i)u(\boldsymbol{x}_j)]\lambda_j + \sum_{l=1}^{m} \mu_l p_l(\boldsymbol{x}_i) = E[u(\boldsymbol{x}_0)u(\boldsymbol{x}_i)], \quad 1\le i\le n \tag{6}$$

$$\sum_{j=1}^{n} \lambda_j p_l(\boldsymbol{x}_j) = p_l(\boldsymbol{x}_0), \quad 1\le l\le k \tag{7}$$

where coefficients μ_l $(1\le l\le k)$ are the Lagrange multipliers associated with the constraints that satisfy the no-bias conditions.

The covariance $E[u(\boldsymbol{x}_0)u(\boldsymbol{x}_i)]$ in Eq. (6) can be expressed by the semivariogram $\gamma(\boldsymbol{h})$ by using the intrinsic hypothesis (Trochu, 1993), i.e.

$$\gamma(\boldsymbol{x}_0, \boldsymbol{x}_i) = \gamma(\boldsymbol{h}) = \frac{1}{2}E\{[u(\boldsymbol{x}_i) - u(\boldsymbol{x}_0)]^2\} \tag{8}$$

where $\boldsymbol{h}$ is the Euclidean distance between $\boldsymbol{x}_0$ and $\boldsymbol{x}_i$. Similarly, the covariance $E[u(\boldsymbol{x}_i)u(\boldsymbol{x}_j)]$ is replaced by $\gamma(\boldsymbol{x}_i, \boldsymbol{x}_j)$.

The Kriging system (Eqs. (6) and (7)) can be rewritten in the matrix form

$$\boldsymbol{G}\boldsymbol{c}=\boldsymbol{g} \tag{9}$$

where

$$G = \begin{bmatrix} \boldsymbol{R} & \boldsymbol{P} \\ \boldsymbol{P}^T & \boldsymbol{0} \end{bmatrix} = \begin{bmatrix} \gamma(\boldsymbol{x}_1, \boldsymbol{x}_1) & \cdots & \gamma(\boldsymbol{x}_1, \boldsymbol{x}_n) & p_1(\boldsymbol{x}_1) & \cdots & p_k(\boldsymbol{x}_1) \\ \cdots & \cdots & \cdots & \cdots & \cdots & \cdots \\ \gamma(\boldsymbol{x}_n, \boldsymbol{x}_1) & \cdots & \gamma(\boldsymbol{x}_n, \boldsymbol{x}_n) & p_1(\boldsymbol{x}_n) & \cdots & p_k(\boldsymbol{x}_n) \\ p_1(\boldsymbol{x}_1) & \cdots & p_1(\boldsymbol{x}_n) & 0 & \cdots & 0 \\ \cdots & \cdots & \cdots & \cdots & \cdots & \cdots \\ p_k(\boldsymbol{x}_1) & \cdots & p_k(\boldsymbol{x}_n) & 0 & \cdots & 0 \end{bmatrix} \tag{10}$$

$$\boldsymbol{c}=\{\lambda_1 \ \cdots \ \lambda_n \ \mu_1 \ \cdots \ \mu_k\}^T \tag{11}$$

$$\boldsymbol{g}=\{\gamma(\boldsymbol{x}_0) \ \boldsymbol{p}(\boldsymbol{x}_0)\}^T = \{\gamma(\boldsymbol{x}_0, \boldsymbol{x}_1) \ \cdots \ \gamma(\boldsymbol{x}_0, \boldsymbol{x}_n) \ p_1(\boldsymbol{x}_0) \ \cdots \ p_k(\boldsymbol{x}_0)\}^T \tag{12}$$

In practical applications, several semivariogram models have been proposed and used (Olea, 1999). Among them, the Gaussian semivariogram model is widely used and leads to good results for problems in computational mechanics (Liu *et al*., 2002a; Gu, 2003). Therefore, it is also employed in this paper

$$\gamma(h) = c_0\left(1 - e^{-3(\frac{h}{a_0})^2}\right) \tag{13}$$

where h is the lag, c_0 and a_0 are the sill and range, respectively. The sill c_0 represents the average variance of points at such a distance away from the considered point that there is no correlation between the points. The range a_0 represents the distance at which there is no longer a correlation between the points. A practical rule is to determine the range to be the distance, for which the semivariogram is 0.95 c_0.

Substituting the weights λ_i solved from Eq. (9) into Eq. (1), the estimated value can be obtained and written in the following form (Stein, 1999)

$$u^h(\boldsymbol{x}, \boldsymbol{x}_0)=\boldsymbol{\Phi}(\boldsymbol{x})\boldsymbol{u} \tag{14}$$

where $\boldsymbol{u}=\{\boldsymbol{u}(\boldsymbol{x}_1) \ \boldsymbol{u}(\boldsymbol{x}_2) \ \cdots \ \boldsymbol{u}(\boldsymbol{x}_n)\}^T$, and $\boldsymbol{\Phi}(\boldsymbol{x})$ is defined as the shape function matrix, which can be written as

$$\boldsymbol{\Phi}(\boldsymbol{x})=\boldsymbol{\gamma}(\boldsymbol{x}_0)^T\boldsymbol{S}+\boldsymbol{p}(\boldsymbol{x}_0)^T\boldsymbol{Y} \tag{15}$$

where

$$\boldsymbol{S}=\boldsymbol{R}^{-1}(\boldsymbol{I}-\boldsymbol{P}\boldsymbol{Y}) \tag{16}$$

$$\boldsymbol{Y}=(\boldsymbol{P}^T\boldsymbol{R}^{-1}\boldsymbol{P})^{-1}\boldsymbol{P}^T\boldsymbol{R}^{-1} \tag{17}$$

Then, the estimation variance can be easily computed by

$$s_e^2(\boldsymbol{x}_0) = \sum_{i=1}^{n} \lambda_i \gamma(\boldsymbol{x}_0, \boldsymbol{x}_i) - \sum_{l=1}^{k} \mu_l p_l(\boldsymbol{x}_0) \tag{18}$$

The estimation of variance is useful in the field of statistics, and it has been extended to many other fields. In our work, the scattered points for the interpolation can be considered as random inputs or parameters, the estimation of variance computed by Eq. (18) is a useful indicator to estimate and control the error of the interpolation.

Figure 1 plots the one-dimensional shape functions constructed by Kriging interpolation. It can be found that the Kriging interpolation is a passing node interpolation, and the shape functions derived from it possess the delta function property, i.e.

$$\phi_i(\boldsymbol{x}_j) = \delta_{ij} = \begin{cases} 1 & (i = j,\ i = 1\sim n) \\ 0 & (i \neq j,\ i,\ j = 1\sim n) \end{cases} \tag{19}$$

and satisfy the partition of unity,

$$\sum_{i=1}^{n} \phi_i(\boldsymbol{x}_i) = 1 \tag{20}$$

Equations (19) and (20) are the delta function property and the partition of unity of the Kriging shape functions. They can be obtained from the nature of the Kriging interpolation, and proven by the reproduction properties of the meshfree shape functions (Liu, 2002). The detailed demonstrations can be found in (Gu, 2003; Liu, 2002; Stein, 1999).

III. MESHLESS FORMULATION FOR THE ANALYSIS OF MEMS DEVICES

1. Governing Equation of MEMS Devices

In this paper, the static and dynamic behaviors of MEMS devices are simulated. Two MEMS devices, the microswitch and microtweezer, are considered.

The microswitch is composed of a pair of electrodes. One electrode is rigid and fixed. The other is a deformable elastic structure. When a potential difference (applied voltage) is applied, the elastic structure will close to the fixed electrode. This creates an electrostatic force and causes the contact between the electrodes. The electrostatic pull-in characteristic is important in the analysis, which is a sharp instability in the behavior of an elastically supported structure subjected to parallel-plate electrostatic actuation (Osterberg and Senturia, 1997).

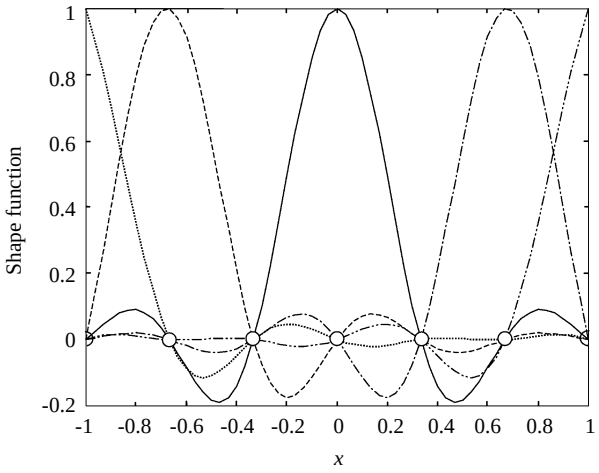

Fig. 1 Shape functions in one-dimensional space

The Microtweezer is a novel application of MEMS technology. It can be used as a microgripper, which could be the fingers of the microtelerobot. The microtweezer was designed and fabricated by MacDonald *et al*. (1989), and studied by Shi *et al*. (1995). The microtweezer comprises two arms, which are rigidly attached at one end but free at the other. Each arm is conformally coated with a thin layer of insulating material to prevent shorting upon closure. When an applied voltage is applied between the arms, they will attract each other. When the applied voltage reaches a value, the two arms will touch each other and the microtweezer is closed.

According to the geometry and deflection character of the microswitch and the microtweezer, they are simplified as 1-D beam structures governed by the Timoshenko beam theory. Neglecting the damping effect, the governing equation of MEMS devices is written as (Reddy, 1993)

$$\begin{cases} \rho A\dfrac{\partial^2 w}{\partial t^2} - \dfrac{\partial}{\partial x}[GAk_s(\dfrac{\partial w}{\partial x} + \theta)] - f = 0 \\ \rho I\dfrac{\partial^2 \theta}{\partial t^2} - \dfrac{\partial}{\partial x}(EI\dfrac{\partial \theta}{\partial x}) + GAk_s(\dfrac{\partial w}{\partial x} + \theta)] = 0 \end{cases}$$

$$\text{in domain } \Omega \tag{21}$$

where w is the deflection of the device, θ the rotation, ρ the mass density, E the modulus of elasticity, I the

moment of inertia, A the cross section area, G the shear modulus, and k_s the shear correction coefficient. f is the external loading.

The boundary conditions for the fixed end of a device (assuming at $x=x_0$) are

$$\begin{cases} w(x_0) = \overline{w} = 0\,, & \text{on } \Gamma_w \\ \theta(x_0) = \overline{\theta} = 0\,, & \text{on } \Gamma_\theta \end{cases} \tag{22}$$

For the free end of a device (assuming at $x=x_0$), they are

$$\begin{cases} M(x_0) = EI\dfrac{\partial\theta}{\partial x}\Big|_{x=x_0} = \overline{M} = 0\,, & \text{on } \Gamma_M \\ Q(x_0) = GAk_s(\theta + \dfrac{\partial w}{\partial x}\Big|_{x=x_0} = \overline{Q} = 0\,, & \text{on } \Gamma_Q \end{cases} \tag{23}$$

where Γ_w, Γ_θ, Γ_M and Γ_Q are the corresponding boundaries of the deflection w, rotation θ, moment M, and force Q prescribed, respectively.

The initial conditions (at $t=t_0$) can be written as

$$\begin{cases} w(x, t_0) = w_0(x)\,, \\ \theta(x, t_0) = \theta_0(x)\,, \\ \dfrac{\partial w(x, t_0)}{\partial t} = \hat{w}_0(x)\,, \\ \dfrac{\partial \theta(x, t_0)}{\partial t} = \hat{\theta}_0(x)\,, \end{cases} \text{ in domain } \Omega \tag{24}$$

2. Local Weak Form

Using the weighted residual technique in a local support domain Ω_s bounded by Γ_s, we obtain the local weak form of Eq. (21) as follows:

$$\begin{cases} \displaystyle\int_{\Omega_s} v\{\rho A\frac{\partial^2 w}{\partial t^2} - \frac{\partial}{\partial x}[GAk_s(\frac{\partial w}{\partial x} + \theta)] - f\}d\Omega = 0 \\ \displaystyle\int_{\Omega_s} v\{\rho I\frac{\partial^2 \theta}{\partial t^2} - \frac{\partial}{\partial x}(EI\frac{\partial \theta}{\partial x}) + GAk_s(\frac{\partial w}{\partial x} + \theta)]d\Omega = 0 \end{cases} \tag{25}$$

where v is the weight function.

Integrating Eq. (25) by parts, we have

$$\begin{cases} \displaystyle\int_{\Omega_s} v\rho A\frac{\partial^2 w}{\partial t^2}d\Omega + \int_{\Omega_s}[\frac{dv}{dx}GAk_s(\frac{\partial w}{\partial x} + \theta) - vf]d\Omega - [\overline{n}\,vGAk_s(\frac{\partial w}{\partial x} + \theta)]\Big|_{\Gamma_s} = 0 \\ \displaystyle\int_{\Omega_s} v\rho I\frac{\partial^2 \theta}{\partial t^2}d\Omega + \int_{\Omega_s}[\frac{dv}{dx}(EI\frac{\partial \theta}{\partial x}) + vGAk_s(\frac{\partial w}{\partial x} + \theta)]d\Omega - [\overline{n}\,v(EI\frac{\partial \theta}{\partial x})]\Big|_{\Gamma_s} = 0 \end{cases} \tag{26}$$

where $\overline{n}$ is the unit outward normal to the domain Ω_s. In implementation, the boundary Γ_s is usually separated into five parts (Gu and Liu, 2001b), which are the internal boundary Γ_{si}, the boundaries Γ_{sw}, $\Gamma_{s\theta}$, Γ_{sM}, and Γ_{sQ}, over which the essential boundary conditions w, θ and natural boundary conditions M, Q are specified, respectively.

In the local weak form (Eq. (25) or (26)), there exist two types of functions, the trial function and weight function. In this paper, the trial function is constructed by the Kriging interpolation (see section II). The 4th order spline function is used as the weight function. The reason is that compared with the quadric and cubic spline function, the 4th order spline function has higher continuity and simpler form. In addition, it can be easily constructed with zero value on the boundary. Therefore, the 4th order spline function is adopted in this paper, i.e.

$$v_i(x) = \begin{cases} 1 - 6(\dfrac{d_i}{r_v})^2 + 8(\dfrac{d_i}{r_v})^3 - 3(\dfrac{d_i}{r_v})^4\,, & 0 \le d_i \le r_v \\ 0\,, & d_i \ge r_v \end{cases} \tag{27}$$

where $d_i=|x_i-x|$ is the distance from node x_i to point x, and r_v is the size of the local support domain.

3. Discrete Formulation

In the Timoshenko beam theory, the deflection w and rotation θ are independent variables, so they

are separately discretized in the space domain, that is

$$\begin{cases} w(x, t) = \boldsymbol{\Phi}^{w}(x)\boldsymbol{w}_e(t) \\ \theta(x, t) = \boldsymbol{\Phi}^{\theta}(x)\boldsymbol{\theta}_e(t) \end{cases} \tag{28}$$

where $\boldsymbol{\Phi}^{w}(x)$ and $\boldsymbol{\Phi}^{\theta}(x)$ are shape functions corresponding to the deflection and the rotation, respectively, which can be computed from Eq. (15). $\boldsymbol{w}_e(t)$ and $\boldsymbol{\theta}_e(t)$ are the nodal deflections and rotations, which are functions of time t.

Applying Eq. (28) in Eq. (26) for all nodes in the whole domain Ω, we can obtain the discretized equations. They can be written as the following form

$$\boldsymbol{M}\ddot{\boldsymbol{u}}(t)+\boldsymbol{K}\boldsymbol{u}(t)=\boldsymbol{f}(t) \tag{29}$$

where $\boldsymbol{M}$ and $\boldsymbol{K}$ are the mass matrix and stiffness matrix, respectively. $\boldsymbol{u}(t)$ is the vector of nodal deflections and rotations at time t, i.e. $\boldsymbol{u}(t)=\{w_1 \ \ \theta_1 \ \ \ldots \ w_N \ \ \theta_N\}^T$, where N is the total node number in Ω. $\ddot{\boldsymbol{u}}(t)$ is the accelerator vector, and $\boldsymbol{f}(t)$ is the vector of external force.

The elements of matrixes $\boldsymbol{M}$, $\boldsymbol{K}$, and vector $\boldsymbol{f}$ can be written as

$$m_{ij}^{11} = \int_{\Omega_s} \rho A v_i \Phi_j^{w} d\Omega$$

$$m_{ij}^{12} = m_{ij}^{21} = 0$$

$$m_{ij}^{22} = \int_{\Omega_s} \rho I v_i \Phi_j^{\theta} d\Omega$$

$$k_{ij}^{11} = \int_{\Omega_s} GAk_s \frac{dv_i}{dx}\frac{d\Phi_j^{w}}{dx} d\Omega - [\overline{n} GAk_s v_i \frac{d\Phi_j^{w}}{dx}]\Big|_{\Gamma_{si}+\Gamma_{sw}+\Gamma_{s\theta}+\Gamma_{sM}}$$

$$k_{ij}^{12} = \int_{\Omega_s} GAk_s \frac{dv_i}{dx}\Phi_j^{\theta} d\Omega - [\overline{n} GAk_s v_i \Phi_j^{\theta}]\Big|_{\Gamma_{si}+\Gamma_{sw}+\Gamma_{s\theta}+\Gamma_{sM}}$$

$$k_{ij}^{21} = \int_{\Omega_s} GAk_s v_i \frac{d\Phi_j^{w}}{dx} d\Omega$$

$$k_{ij}^{22} = \int_{\Omega_s} (EI\frac{dv_i}{dx}\frac{d\Phi_j^{\theta}}{dx} + GAk_s v_i \Phi_j^{\theta}) d\Omega - [\overline{n} EIv_i \frac{d\Phi_j^{\theta}}{dx}]\Big|_{\Gamma_{si}+\Gamma_{sw}+\Gamma_{s\theta}+\Gamma_{sV}}$$

$$f_i^{w} = \int_{\Omega_s} v_i f d\Omega + [\overline{n} v_i \overline{V}]\Big|_{\Gamma_{sV}}$$

$$f_i^{\theta} = [\overline{n} v_i \overline{M}]\Big|_{\Gamma_{sM}} \tag{30}$$

where i, j=1~N.

The dynamic system Eq. (29) is solved by the standard Newmark method (Reddy, 1993).

4. The Nonlinear Loading and Iteration Technique

In Eq. (21), f is the external loading. If f is a linear load, Eq. (29) can be solved by the standard Newmark method. In the simulation of the microswitch and microtweezer, the external loading f in Eq. (21) is nonlinear. It is the function of the deflection and takes the following form (Osterberg and Senturia, 1997)

$$f = -\frac{\varepsilon_0 V^2 b}{2g^2}(1 + 0.65\frac{g}{b}) \quad \text{for static case}$$

$$f = -\frac{\varepsilon_0 V^2 b}{2g^2}(1 + 0.65\frac{g}{b}) \cdot k(t) \quad \text{for dynamic case} \tag{31}$$

where ε_0 is the permittivity of vacuum, V applied voltage, b beam width, and g the gap between the beam and the electrode, i.e. $g=g_0-w(x, t)$, where g_0 is the distance between the initial position of the MEMS device and the electrode. In Eq. (31), the time function $k(t)$ is considered as a constant 1.0.

It can be found from Eq. (31), the force acting on the device is the function of the deflection, i.e., non-linear loading. The nonlinear force f leads to the nonlinearity of Eq. (29). The common solver for linear equations cannot be used. Therefore, the iteration technique is required to solve this non-linear equation. The iteration is performed in each time step, and the iteration criteria is

$$\sqrt{\sum_{j=1}^{N} (w_j^{i+1} - w_j^{i})^2} \le e \tag{32}$$

where N is the number of nodes used, w_j^i and w_j^{i+1} are the deflections of the ith and (i+1)th iteration steps, respectively. e is a specified accuracy tolerance.

IV. RESULTS AND DISCUSSIONS

To prove the efficiency, the present LoKringing meshless method is first tested on two benchmark problems, and then the present method is used to analyze the static and dynamic behaviors of MEMS devices, i.e. the microswitch and microtweezer.

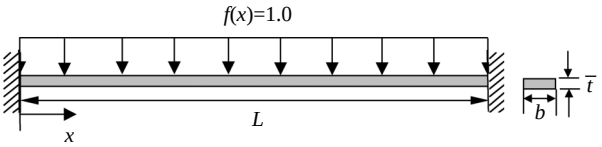

Fig. 2 A fixed-fixed thin beam under uniform loading

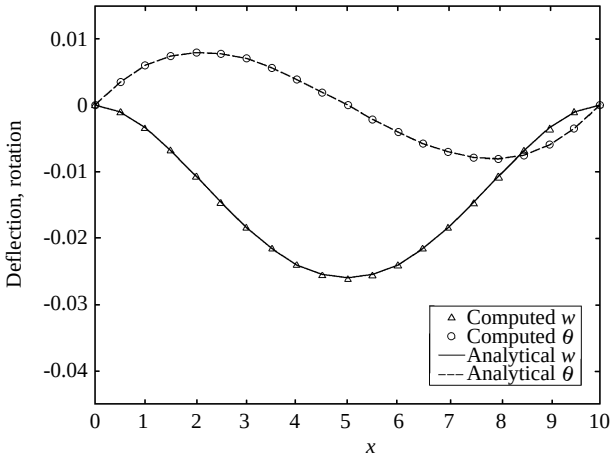

Fig. 3 Deflection and rotation results of the fixed-fixed thin beam

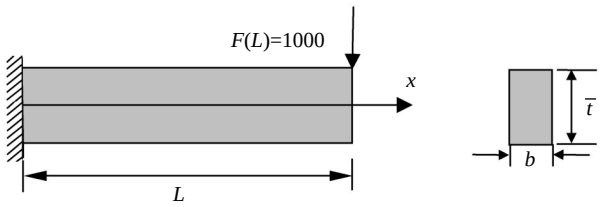

Fig. 4 A cantilever thick beam under concentrated loading

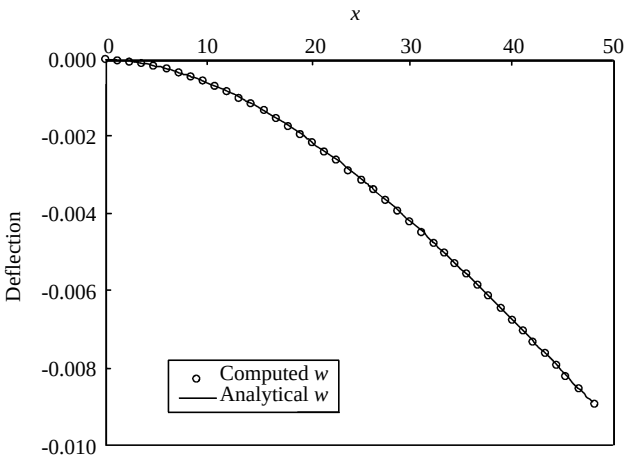

Fig. 5 Deflection results of the cantilever thick beam

1. Benchmark Problems

(i) Fixed-Fixed Thin Beam

When the ratio of the length to thickness of the beam is larger (i.e. more than 5~10), it is usually defined as a thin beam shown in Fig. 2. The parameters of the thin beam studied in this example are: L=10 (length), b=1.0 (width), and $\overline{t}$ =0.1 (thickness). The ratio of the length to thickness is 100. The Young's modulus is 1.2×10^7, the Poisson ratio is 0.3, and the uniform distributed loading $f(x)$=1.0. The beam is discretized by 21 uniformly distributed nodes. The static deflections and rotations of the beam are computed and plotted in Fig. 3. They are compared with the analytical solution of Bernoulli-Euler beam theory (Timoshenko, 1955). It is shown that the computed results and the analytical solution agree very well.

In practical applications, when a thin beam is studied by thick beam theory, there usually exists a shear-locking phenomenon, which leads to incorrect results. To avoid this phenomenon, some special techniques have been developed, such as adding the transverse shear strain as another variable (Cho *et al.*, 2000), using the high order shape functions (Liu, 2002), and so on. In Fig. 3, it can be seen that the shear-locking phenomenon has been avoided successfully by the LoKriging method. It is because the shape functions constructed by the Kriging interpolation have high order.

(ii) Cantilever Thick Beam

When the ratio of the length to thickness of the beam is smaller (less than 5), thick beam theory, in which the shear effect is considered, should be used. As shown in Fig. 4, the parameters of the thick beam are: L=48 (length), b=1.0 (width), and $\overline{t}$ =12 (thickness). The Young's modulus is 3.0×10^7, the Poisson ratio is 0.3, and the concentrated loading $F(L)$=1000. Because the ratio of the length to thickness is only 4, this beam is a thick beam.

A total of 21 uniformly distributed nodes are used to discretize the beam. The computed static deflections of the beam are compared with the analytical solution (Timoshenko and Goodier, 1970) in Fig. 5. It is found that the present LoKriging method leads to a very good result.

2. Microswitch

As shown in Fig. 6, a widely used MEMS device, a microswitch, is considered. The dimension of the microswitch is 80 μm long, 10 μm wide and 0.5 μm thick. The initial gap, g_0, between the switch and the electrode is 0.7 μm. The Young's modulus E is 169 GPa, and the mass density ρ is 2231 kg/m^3 (Ananthasuresh *et al.*, 1996). It is simplified as a fixed-fixed beam, as shown in Fig. 6, and it is

Table 1 Comparison of the critical pull-in volatge of the microswitch between the present method and other methods

	Experimental method (Ananthasuresh *et al.*, 1996) (volt)	*v*LPIM (Li *et al.*, 2003) (volt)	LoKriging method (volt)
Static simulation	15.17	15.1	15.09
Dynamic simulation	13.8	13.8	13.77

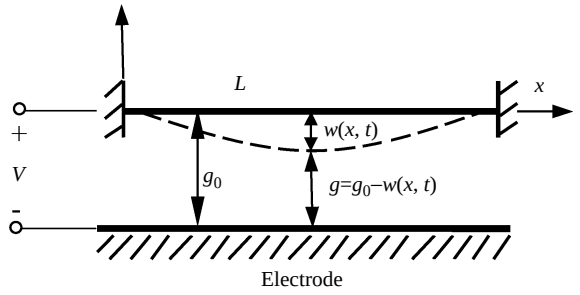

Fig. 6 The microswitch simplified as a fixed-fixed beam

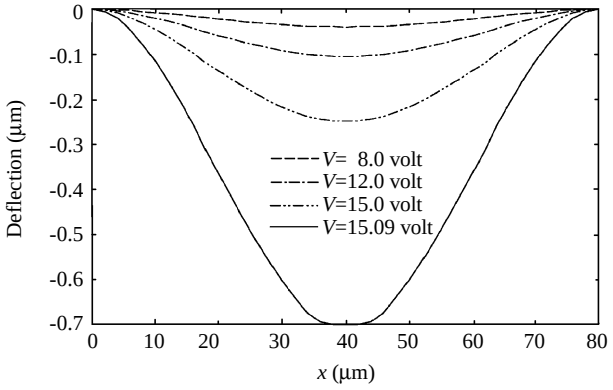

Fig. 7 Static deflection of the microswitch at different applied voltages

discretized by 41 uniformly distributed nodes.

The static behavior of the microswitch is first analyzed by the present LoKriging method. Deflection results of different applied voltage are obtained by the LoKriging method, and plotted in Fig. 7. It is found that when the applied voltage is imposed on the microswitch, it deflects. With the increase of the applied voltage, the deflection of the microswitch increases; the gap between the microswitch and the electrode becomes smaller. When the applied voltage increases to one certain value, defined as the critical pull-in voltage, the microswitch becomes unstable and the centre of the microswitch touches the electrode. For the above mentioned microswitch, the static critical pull-in voltage is 15.09 volts. This result is compared with the experimental (Ananthasuresh *et al.*, 1996) and other numerical (Li *et al.*, 2003) results, and listed in Table 1. It is shown

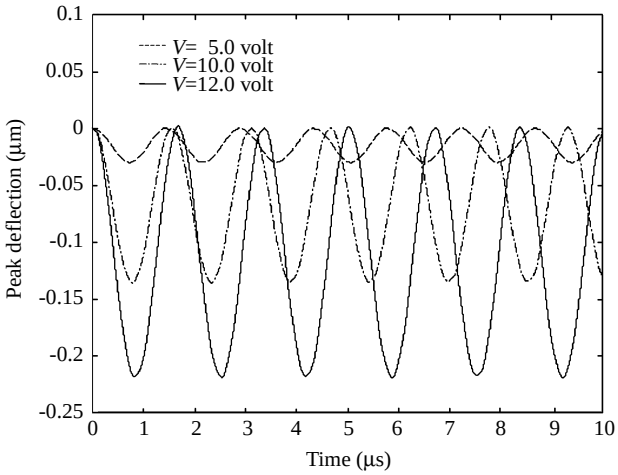

Fig. 8 Dynamic response of the microswitch at different applied voltages

that these results agree very well.

In the dynamic simulation for the microswitch, the time step is taken as $\Delta t=1\times10^{-3}$ μs. Fig. 8 shows the dynamic response of the centre of the microswitch, called peak deflection, under different applied voltages. It can be observed that when the applied voltage increases, the peak defection of the microswitch increases. It can be also found that the fundamental frequency of the microswitch decreases with the increase of the applied voltage. Similar to the static simulation, the dynamic critical pull-in voltage can be obtained. For the same microswitch, the dynamic critical pull-in voltage is 13.77 volts. The dynamic pull-in behavior of the microswitch is plotted in Fig. 9. It can be seen that this process is nonlinear. The comparisons with other simulation results of the dynamic critical pull-in voltages are also listed in Table 1. The error is only 2%. Very good results are obtained. In addition, comparing the static and dynamic critical pull-in voltage, we find that the static value is larger than the dynamic value by about 9%.

3. Microtweezer

As shown in Fig. 10(a), another MEMS device, a microtweezer, is analyzed. The simplified

Table 2 Comparison of the critical closing voltage of the microtweezer between the present method and other methods

	Experimental method (MacDonald, *et al*., 1989) (volt)	FEM (Shi *et al*., 1995) (volt)	LoKriging method (volt)
Static simulation	150	156~157	153
Dynamic simulation	–	–	125.2~125.3

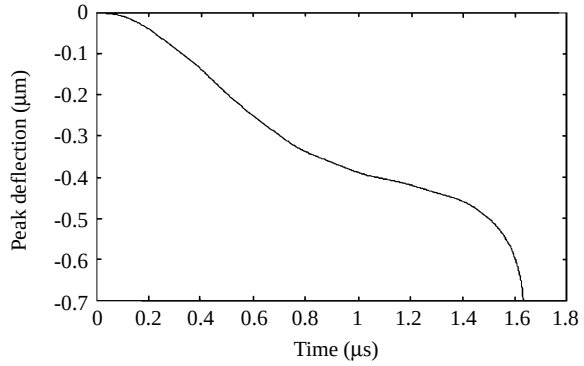

Fig. 9 Dynamic pull-in behavior of the microswitch

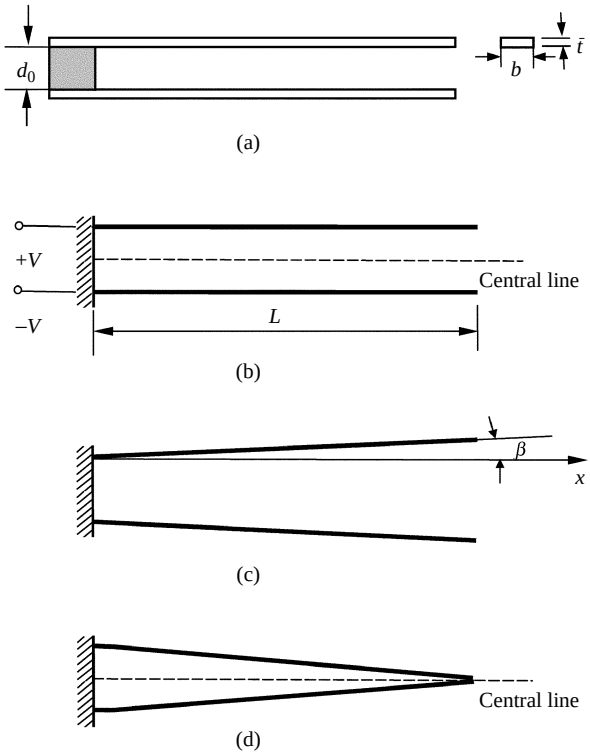

Fig. 10 Microtweezer (a) a simplified microtweezer geometry; (b) microtweezer arms simplified as cantilever beams; (c) microtweezer arms with an angle; (d) microtweezer arms closed

geometry of the tungsten microtweezer is shown in Fig. 10(a). The tweezer arms are simplified as cantilever beams in Fig. 10(b). In the simulation, the effect of the coating layers is neglected.

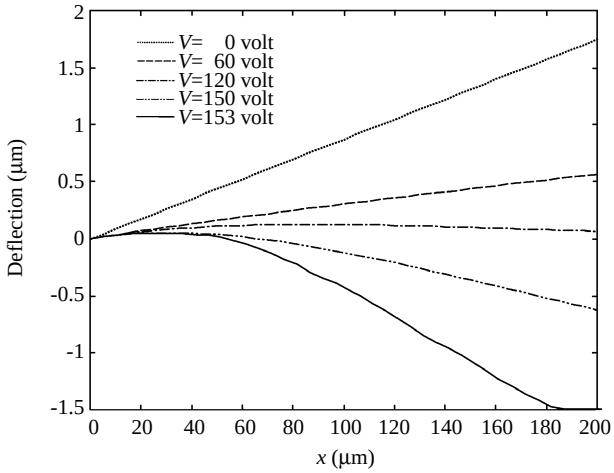

Fig. 11 Deformed shape of the microtweezer arm at different applied voltages

The parameters for the microtweezer arms are: 200 μm long, 2.7 μm wide and 2.5 μm thick. The Young's modulus is 410 GPa, and the mass density ρ is 19300 kg/m^3. The initial opening of the two arms, d_0, is 3 μm. It has been designed and simulated (MacDonald *et al*., 1989; Shi *et al*., 1995).

In practical applications, there may be an initial angle between the arms and the central line of the microtweezer, shown in Fig. 10(c). For generalization, a microtweezer with an initial angle β=0.5° is simulated using the present LoKriging method. When the applied voltage is imposed on the arms, they deflect and move to the central line. As the applied voltage increases, the deflections of the arms become larger. When the voltage reaches one certain value, the tips of two arms contact with each other (As shown in Fig. 10(d)). This critical voltage is defined as pull-in voltage (*closing voltage*). Because of the symmetry of the microtweezer, only one arm is considered in the simulation. The closing voltages for the static and dynamic analyses are summarized in Table 2. The static results agree very well with the experimental and other numerical results.

Figure 11 plots the deflection of the microtweezer arm at different applied voltages. It is observed that when the applied voltage is smaller than 150 volts, the two arms do not contact. When the voltage is increased slightly beyond 150 volt up to

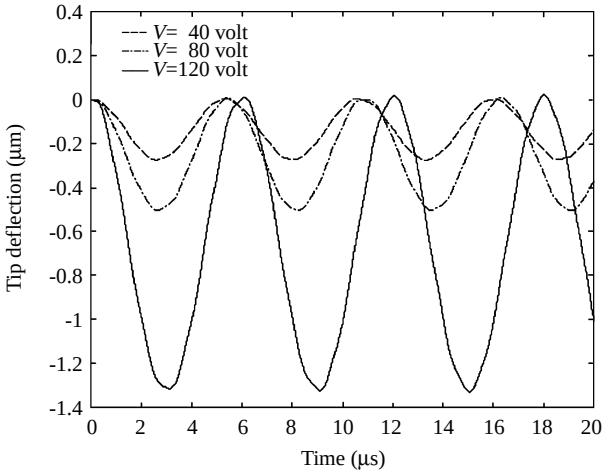

Fig. 12 Dynamic simulation of the microtweezer arm at different applied voltages

153 volt, a large deflection of the arm tip is generated, leading to the contact of the two arms.

The dynamic response of the arm tip is obtained and plotted in Fig. 12. In dynamic analysis, the time step is taken as $\Delta t=1\times10^{-3}$ μs. Similar to the microswitch discussed above, with the increase of the applied voltage, the fundamental frequency decreases. In addition, the dynamic closing voltage is also obtained and listed in Table 2. Compared with the static closing voltage, the dynamic closing voltage is smaller.

V. CONCLUSIONS

A meshless Local Kriging (LoKriging) method is developed for static and dynamic analyses of MEMS devices. In LoKriging, the Kriging interpolation method is used to construct the trial function, and the locally weighted residual technique is used to get the local weak form. The present LoKriging method is used to analyze the characteristics of MEMS structures. The comparisons between the computed results and the experimental or other numerical results show that the present method is efficient and accurate to solve MEMS structures.

It should be mentioned here that although the MEMS devices are simplified as beam structures in this paper, there are many MEMS devices with very complex geometry in practical applications. Because of the efficiency, accuracy and stability of the LoKriging method, the present LoKriging method has very good potential for simulations of practical complex MEMS devices (for example a MEMS device with a plate structure). Of course, further research is required.

REFERENCES

Ananthasuresh, G. K., Gupta, R. K., and Senturia, S. D., 1996, "An Approach to Macromodeling of MEMS for Nonlinear Dynamic Simulation. Microelectromechanical Systems (MEMS)," *ASME Dynamic Systems and Control (DSC) Series*, Vol. 59, pp. 401-407.

Atluri, S. N., and Zhu, T., 1998, "A New Meshless Local Petrov-Galerkin (MLPG) Approach in Computational Mechanics," *Computational Mechanics*, Vol. 22, No. 2, pp. 117-127.

Atluri, S. N., Cho, J. Y., and Kim, H. G., 1999a, "Analysis of Thin Beams, Using the Meshless Local Petrov-Galerkin (MLPG) Method, with Generalized Moving Least Squares Interpolation," *Computational Mechanics*, Vol. 24, No. 5, pp. 334-347.

Atluri, S. N., Kim, H. G., and Cho, J. Y., 1999b, "A Critical Assessment of the Truly Meshless Local Petrov-Galerkin (MLPG), and Local Boundary Integral Equation (LBIE) Methods," *Computational Mechanics*, Vol. 24, No. 5, pp. 348-372.

Belytschko, T., Krongauz, Y., Organ, D., Fleming, M., and Krysl, P., 1996, "Meshless Methods: An Over-View and Recent Developments," *Computer Methods in Applied Mechanics and Engineering*, Vol. 139, Nos. 1-4, pp. 3-47.

Belytschko, T., Lu, Y. Y., and Gu, L., 1994, "Element-Free Galerkin Methods," *International Journal for Numerical Methods in Engineering*, Vol. 37, pp. 229-256.

Bernard, P. S., 1995, "A Deterministic Vortex Sheet Method for Boundary Layer Flow," *Journal of Computational Physics*, Vol. 117, No. 1, pp. 132-145.

Cho, J. Y., Kim, H. G., and Atluri, S. N., 2000, "Analysis of Shear Flexible Beams, Using the Meshless Local Petrov-Galerkin Method Based on Locking-Free Formulation," *Proceedings of Advances in Computational Engineering and Science*, Los Angeles, pp. 1404-1409.

Gingold, R. A., and Monaghan, J. J., 1977, "Smooth Particle Hydrodynamics: Theory and Applications to Non-Spherical Stars," *Monthly Notices of the Royal Astronomical Society*, Vol. 181, pp. 375-389.

Gu, L., 2003, "Moving Kriging Interpolation and Element-Free Galerkin Method," *International Journal for Numerical Methods in Engineering*, Vol. 56, No. 1, pp. 1-11.

Gu, Y. T., and Liu, G. R., 2001a, "A Meshless Local Petrov-Galerkin (MLPG) Method for Free and Forced Vibration Analyses for Solids," *Computational Mechanics*, Vol. 27, No. 3, pp. 188-198.

Gu, Y. T., and Liu, G. R., 2001b, "A Local Point Interpolation Method for Static and Dynamic Analysis of Thin Beams," *Computer Methods in Applied Mechanics and Engineering*, Vol. 190, No.

42, pp. 5515-5528.

Hung, E. S., and Senturia, S. D., 1999, "Generating Efficient Dynamical Models for Microelectromechanical Systems from a Few Finite-Element Simulation Runs," *IEEE Journal of Microelectromechanical Systems*, Vol. 8, No. 3, pp. 280-289.

Krige, D. G., 1951, "A Statistical Approach to Some Basic Mine Valuation Problems on the Witwatersand," *Journal of the Chemical, Metallurgical and Mining Society of South Africa*, Vol. 52, pp. 119-139.

Krige, D. G., 1976, "A Review of the Development of Geostatistics in South Africa," in: David, M., Huijbregts, C., ed., *Advanced Geostatistcs in the Mining Industry*, pp. 279-293.

Leonard, A., 1980, "Vortex Methods for Flow Simulation," *Journal of Computational Mechanics*, Vol. 37, pp. 289-335.

Li, Hua, Wang, Q. X., and Lam, K. Y., 2003, "A Variation of Local Point Interpolation Method (*v*LPIM) for Analysis of Microelectromechanical Systems (MEMS) Device," *Engineering Analysis with Boundary Elements* (accepted).

Liszka, T., 1984, "An Interpolation Method for an Irregular Net of Nodes," *International Journal for Numerical Methods in Engineering*, Vol. 20, pp. 1599-1612.

Liu, G. R., 2002, *Meshfree Methods: Moving Beyond the Finite Element Method*, CRC press, Boca Raton, FL, USA.

Liu, G. R., Dai, K. Y., Gu, Y. T., and Lim, K. M., 2002b, "A Comparison between Radial Point Interpolation Method (RPIM) and Kriging Based Meshfree Method," *Advances in Meshfree and X-FEM Methods, Proceeding of the 1st Asian workshop on meshfree methods*, Singapore, pp. 29-34.

Liu, G. R., and Gu, Y. T., 2001a, "A Point Interpolation Method for Two-Dimensional Solid," *International Journal for Numerical Methods in Engineering*, Vol. 50, No. 4, pp. 937-951.

Liu, G. R., and Gu, Y. T., 2001b, "A Local Radial Point Interpolation Method (LR-PIM) for Free Vibration Analyses of 2-D Solids," *Journal of Sound and Vibration*, Vol. 246, No. 1, pp. 29-46.

Liu, G. R., Yan, L., Wang, J. G., and Gu, Y. T., 2002a, "Point Interpolation Method Based on Local Residual Formulation Using Radial Basis Functions, " *Structural Engineering and Mechanics*, Vol. 14, No. 6, pp. 713-732.

Lyshevski, S. E., 2002, *MEMS and NEMS Systems, Devices, and Structures*, CRC Press, Boca Raton, FL, USA.

MacDonald, N. C., Chen, L. Y., Yao, J. J., Zhang, J. A., Mcmillan, J. A., and Thomas, D. C., 1989, "Selective Chemical Vapor Deposition of Tungsten for Microelectomechanical Structures," *Sensors and Actuators*, Vol. 20, pp. 123-133.

Monaghan, J. J., 1985, "Particle Methods for Hydrodynamics," *Computer Physics Report*, Vol. 3, pp. 71-1246.

Olea, R. A., 1999, *Geostatistics for Engineers and Earth Scientists*, Kluwer Academic Publishers, Boston, MA, USA.

Osterberg, P. M., and Senturia, S. D., 1997, "M-TEST: A Test Chip for MEMS Material Property Measurement Using Electrostatically Actuated Test structures," *Journal of Microelectromechanical Systems*, Vol. 6, No. 2, pp. 107-118.

Reddy, J. N., 1993, *An introduction to the finite element method*, 2nd ed., McGraw Hill, New York, USA.

Sacks, J., Welch, W. J., Mitchell, T. J., and Wynn, H. P., 1989, "Design and Analysis of Computer Experiments," *Statistical Science*, Vol. 4, pp. 409-435.

Senturia, S, D., 1998, "CAD Challenges for Microsensors, Microactuators, and Microsystems," *Proceedings of the IEEE*, Vol. 86, No. 8, pp. 1611-1626.

Shi, F., Ramesh, P., and Mukherjee, S., 1995, "Simulation Methods for Micro-Electro-Mechanical Structures (MEMS) with Application to a Microtweezer," *Computers and Structures*, Vol. 56, No. 5, pp. 769-783.

Simpson, T. W., Mauery, T. M., Korte, J. J., and Mistree, F., 1998, "Comparison of Response Surface and Kriging Models for Multidisciplinary Design Optimization," *Proceedings of the 7th Symposium on Multidisciplinary Analysis and Optimization*, *AIAA*-98-4755.

Stein, M. L., 1999, *Interpolation of Spatial Data-Some Theory for Kriging*, Springer, New York, USA.

Timoshenko, S. P., 1955, *Strength of Materials*, D. Van Nostrand Co., Princeton, NJ, USA.

Timoshenko, S. P., and Goodier, J. N., 1970, *Theory of Elasticity*, 3rd ed., McGraw-hill, New York, USA.

Trochu, F., 1993, "A Contouring Program Based on Dual Kriging Iinterpolation," *Engineering with Computers*, Vol. 9, pp. 160-177.

Manuscript Received: Aug. 05, 2003
Revision Received: Jan. 29, 2004
and Accepted: Mar. 01, 2004